(b) Implement a histogram filter and run its prediction step. Compare the resulting posterior with the one from the EKF and from your intuitive analysis. What can you learn about the resolution of the x-y coordinates and the orientation θ in your histogram filter?

(c) Now incorporate a measurement into your estimate. As before, the measurement shall be a noisy projection of the x-coordinate of the robot, with covariance $Q = 0.01$. Implement the step, compute the result, plot it, and compare it with the result of the EKF and your intuitive drawing.

Notice: When plotting the result of a histogram filter, you can show multiple density plots, one for each discrete slice in the space of all θ-values.

3. We talked about the effect of using a single particle. What is the effect of using $M = 2$ particles in particle filtering? Can you give an example where the posterior will be biased? If so, by what amount?

4. Implement Exercise 1 using particle filters instead of histograms, and plot and discuss the results.

5. Implement Exercise 2 using particle filters instead of histograms, and plot and discuss the results. Investigate the effect of varying numbers of particles on the result.

5 Robot Motion

5.1 Introduction

This and the next chapter describe the two remaining components for implementing the filter algorithms described thus far: the motion and the measurement models. This chapter focuses on the motion model. *Motion models* comprise the state transition probability $p(x_t \mid u_t, x_{t-1})$, which plays an essential role in the prediction step of the Bayes filter. This chapter provides in-depth examples of probabilistic motion models as they are being used in actual robotics implementations. The subsequent chapter will describe probabilistic models of sensor measurements $p(z_t \mid x_t)$, which are essential for the measurement update step. The material presented here will be essential for *implementing* any of the algorithms described in subsequent chapters.

Robot kinematics, which is the central topic of this chapter, has been studied thoroughly in past decades. However, it has almost exclusively been addressed in deterministic form. Probabilistic robotics generalizes kinematic equations to the fact that the outcome of a control is uncertain, due to control noise or unmodeled exogenous effects. Following the theme of this book, our description will be probabilistic: The outcome of a control will be described by a posterior probability. In doing so, the resulting models will be amenable to the probabilistic state estimation techniques described in the previous chapters.

Our exposition focuses entirely on mobile robot kinematics for robots operating in planar environments. In this way, it is much more specific than most contemporary treatments of kinematics. No model of manipulator kinematics will be provided, neither will we discuss models of robot dynamics. However, this restricted choice of material is by no means to be interpreted that probabilistic ideas are limited to simple kinematic models of

mobile robots. Rather, it is descriptive of the present state of the art, as probabilistic techniques have enjoyed their biggest successes in mobile robotics using relatively basic models of the types described in this chapter. The use of more sophisticated probabilistic models (e.g., probabilistic models of robot dynamics) remains largely unexplored in the literature. Such extensions, however, are not infeasible. As this chapter illustrates, deterministic robot actuator models are "probilified" by adding noise variables that characterize the types of uncertainty that exist in robotic actuation.

In theory, the goal of a proper probabilistic model may appear to accurately model the specific types of uncertainty that exist in robot actuation and perception. In practice, the exact shape of the model often seems to be less important than the fact that some provisions for uncertain outcomes are provided in the first place. In fact, many of the models that have proven most successful in practical applications vastly overestimate the amount of uncertainty. By doing so, the resulting algorithms are more robust to violations of the Markov assumptions (Chapter 2.4.4), such as unmodeled state and the effect of algorithmic approximations. We will point out such findings in later chapters, when discussing actual implementations of probabilistic robotic algorithms.

5.2 Preliminaries

5.2.1 Kinematic Configuration

CONFIGURATION

Kinematics is the calculus describing the effect of control actions on the configuration of a robot. The *configuration* of a rigid mobile robot is commonly described by six variables, its three-dimensional Cartesian coordinates and its three Euler angles (roll, pitch, yaw) relative to an external coordinate frame. The material presented in this book is largely restricted to mobile robots operating in planar environments, whose kinematic state is summarized by three variables, referred to as pose in this text.

POSE

The *pose* of a mobile robot operating in a plane is illustrated in Figure 5.1. It comprises its two-dimensional planar coordinates relative to an external coordinate frame, along with its angular orientation. Denoting the former as x and y (not to be confused with the state variable x_t), and the latter by θ, the

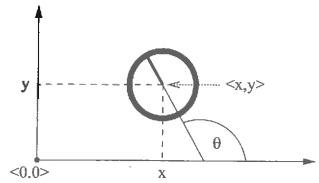

Figure 5.1 Robot pose, shown in a global coordinate system.

pose of the robot is described by the following vector:

$$\begin{pmatrix} x \\ y \\ \theta \end{pmatrix} \tag{5.1}$$

BEARING

The orientation of a robot is often called *bearing*, or *heading direction*. As shown in Figure 5.1, we postulate that a robot with orientation $\theta = 0$ points into the direction of its x-axis. A robot with orientation $\theta = .5\pi$ points into the direction of its y-axis.

LOCATION

Pose without orientation will be called *location*. The concept of location will be important in the next chapter, when we discuss measures to describe robot environments. For simplicity, locations in this book are usually described by two-dimensional vectors, which refer to the x-y coordinates of an object:

$$\begin{pmatrix} x \\ y \end{pmatrix} \tag{5.2}$$

The pose and the locations of objects in the environment may constitute the kinematic state x_t of the robot-environment system.

5.2.2 Probabilistic Kinematics

The probabilistic kinematic model, or *motion model* plays the role of the state transition model in mobile robotics. This model is the familiar conditional density

$$p(x_t \mid u_t, x_{t-1}) \tag{5.3}$$

Here x_t and x_{t-1} are both robot poses (and not just its x-coordinates), and u_t is a motion command. This model describes the posterior distribution

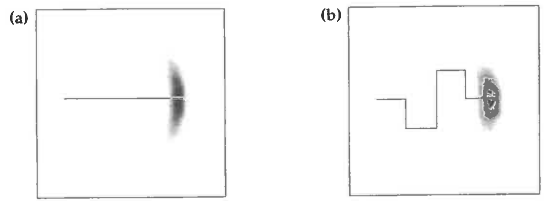

Figure 5.2 The motion model: Posterior distributions of the robot's pose upon executing the motion command illustrated by the solid line. The darker a location, the more likely it is. This plot has been projected into 2-D. The original density is three-dimensional, taking the robot's heading direction θ into account.

over kinematic states that a robot assumes when executing the motion command u_t at x_{t-1}. In implementations, u_t is sometimes provided by a robot's odometry. However, for conceptual reasons we will refer to u_t as control.

Figure 5.2 shows two examples that illustrate the kinematic model for a rigid mobile robot operating in a planar environment. In both cases, the robot's initial pose is x_{t-1}. The distribution $p(x_t \mid u_t, x_{t-1})$ is visualized by the shaded area: The darker a pose, the more likely it is. In this figure, the posterior pose probability is projected into x-y-space; the figure lacks a dimension corresponding to the robot's orientation. In Figure 5.2a, a robot moves forward some distance, during which it may accrue translational and rotational error as indicated. Figure 5.2b shows the resulting distribution of a more complicated motion command, which leads to a larger spread of uncertainty.

This chapter provides in detail two specific probabilistic motion models $p(x_t \mid u_t, x_{t-1})$, both for mobile robots operating in the plane. Both models are somewhat complementary in the type of motion information that is being processed. The first assumes that the motion data u_t specifies the velocity commands given to the robot's motors. Many commercial mobile robots (e.g., differential drive, synchro drive) are actuated by independent translational and rotational velocities, or are best thought of being actuated in this way. The second model assumes that one has access to odometry information. Most commercial bases provide odometry using kinematic information (distance traveled, angle turned). The resulting probabilistic model for integrating such information is somewhat different from the velocity model.

In practice, odometry models tend to be more accurate than velocity models, for the simple reason that most commercial robots do not execute velocity commands with the level of accuracy that can be obtained by measuring the revolution of the robot's wheels. However, odometry is only available after executing a motion command. Hence it cannot be used for motion planning. Planning algorithms such as collision avoidance have to predict the effects of motion. Thus, odometry models are usually applied for estimation, whereas velocity models are used for probabilistic motion planning.

5.3 Velocity Motion Model

The *velocity motion model* assumes that we can control a robot through two velocities, a rotational and a translational velocity. Many commercial robots offer control interfaces where the programmer specifies velocities. Drive trains commonly controlled in this way include differential drives, Ackerman drives, and synchro-drives. Drive systems not covered by our model are those without non-holonomic constraints, such as robots equipped with Mecanum wheels or legged robots.

We will denote the *translational velocity* at time t by v_t, and the *rotational velocity* by ω_t. Hence, we have

$$u_t = \begin{pmatrix} v_t \\ \omega_t \end{pmatrix} \tag{5.4}$$

We arbitrarily postulate that positive rotational velocities ω_t induce a counterclockwise rotation (left turns). Positive translational velocities v_t correspond to forward motion.

5.3.1 Closed Form Calculation

A possible algorithm for computing the probability $p(x_t \mid u_t, x_{t-1})$ is shown in Table 5.1. It accepts as input an initial pose $x_{t-1} = (x \;\; y \;\; \theta)^T$, a control $u_t = (v \;\; \omega)^T$, and a hypothesized successor pose $x_t = (x' \;\; y' \;\; \theta')^T$. It outputs the probability $p(x_t \mid u_t, x_{t-1})$ of being at x_t after executing control u_t beginning in state x_{t-1}, assuming that the control is carried out for the fixed duration Δt. The parameters α_1 to α_6 are robot-specific motion error parameters. The algorithm in Table 5.1 first calculates the controls of an error-free robot; the meaning of the individual variables in this calculation will become more apparent below, when we derive it. These parameters are given by $\hat{v}$ and $\hat{\omega}$.

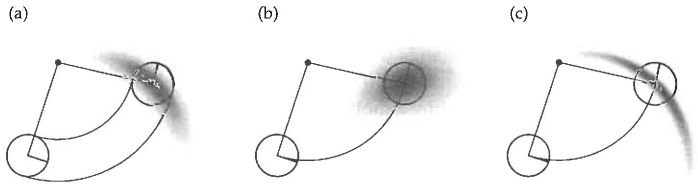

Figure 5.3 The velocity motion model, for different noise parameter settings.

The function $\mathbf{prob}(x, b^2)$ models the motion error. It computes the probability of its parameter x under a zero-centered random variable with variance b^2. Two possible implementations are shown in Table 5.2, for error variables with normal distribution and triangular distribution, respectively.

Figure 5.3 shows graphical examples of the velocity motion model, projected into x-y-space. In all three cases, the robot sets the same translational and angular velocity. Figure 5.3a shows the resulting distribution with moderate error parameters α_1 to α_6. The distribution shown in Figure 5.3b is obtained with smaller angular error (parameters α_3 and α_4) but larger translational error (parameters α_1 and α_2). Figure 5.3c shows the distribution under large angular and small translational error.

5.3.2 Sampling Algorithm

For particle filters (c.f. Chapter 4.3), it suffices to sample from the motion model $p(x_t \mid u_t, x_{t-1})$, instead of computing the posterior for arbitrary x_t, u_t and x_{t-1}. *Sampling* from a conditional density is different than calculating the density: In sampling, one is given u_t and x_{t-1} and seeks to generate a random x_t drawn according to the motion model $p(x_t \mid u_t, x_{t-1})$. When calculating the density, one is also given x_t generated through other means, and one seeks to compute the probability of x_t under $p(x_t \mid u_t, x_{t-1})$.

The algorithm **sample_motion_model_velocity** in Table 5.3 generates random samples from $p(x_t \mid u_t, x_{t-1})$ for a fixed control u_t and pose x_{t-1}. It accepts x_{t-1} and u_t as input and generates a random pose x_t according to the distribution $p(x_t \mid u_t, x_{t-1})$. Line 2 through 4 "perturb" the commanded control parameters by noise, drawn from the error parameters of the kinematic motion model. The noise values are then used to generate the sample's

1:	**Algorithm motion_model_velocity**(x_t, u_t, x_{t-1})**:**
2:	$\mu = \frac{1}{2}\frac{(x-x')\cos\theta + (y-y')\sin\theta}{(y-y')\cos\theta - (x-x')\sin\theta}$
3:	$x^* = \frac{x+x'}{2} + \mu(y-y')$
4:	$y^* = \frac{y+y'}{2} + \mu(x'-x)$
5:	$r^* = \sqrt{(x-x^*)^2 + (y-y^*)^2}$
6:	$\Delta\theta = \text{atan2}(y'-y^*, x'-x^*) - \text{atan2}(y-y^*, x-x^*)$
7:	$\hat{v} = \frac{\Delta\theta}{\Delta t} r^*$
8:	$\hat{\omega} = \frac{\Delta\theta}{\Delta t}$
9:	$\hat{\gamma} = \frac{\theta'-\theta}{\Delta t} - \hat{\omega}$
10:	*return* $\mathbf{prob}(v-\hat{v}, \alpha_1 v^2 + \alpha_2\omega^2) \cdot \mathbf{prob}(\omega-\hat{\omega}, \alpha_3 v^2 + \alpha_4\omega^2)$ $\cdot\, \mathbf{prob}(\hat{\gamma}, \alpha_5 v^2 + \alpha_6\omega^2)$

Table 5.1 Algorithm for computing $p(x_t \mid u_t, x_{t-1})$ based on velocity information. Here we assume x_{t-1} is represented by the vector $(x \;\; y \;\; \theta)^T$; x_t is represented by $(x' \;\; y' \;\; \theta')^T$; and u_t is represented by the velocity vector $(v \;\; \omega)^T$. The function $\mathbf{prob}(a, b^2)$ computes the probability of its argument a under a zero-centered distribution with variance b^2. It may be implemented using any of the algorithms in Table 5.2.

1:	**Algorithm prob_normal_distribution**(a, b^2)**:**
2:	*return* $\frac{1}{\sqrt{2\pi\, b^2}} \exp\left\{-\frac{1}{2}\frac{a^2}{b^2}\right\}$
3:	**Algorithm prob_triangular_distribution**(a, b^2)**:**
4:	*return* $\max\left\{0, \frac{1}{\sqrt{6}\, b} - \frac{\lvert a\rvert}{6\, b^2}\right\}$

Table 5.2 Algorithms for computing densities of a zero-centered normal distribution and a triangular distribution with variance b^2.

1: **Algorithm sample_motion_model_velocity**(u_t, x_{t-1})**:**

2: $\hat{v} = v + \textbf{sample}(\alpha_1 v^2 + \alpha_2 \omega^2)$

3: $\hat{\omega} = \omega + \textbf{sample}(\alpha_3 v^2 + \alpha_4 \omega^2)$

4: $\hat{\gamma} = \textbf{sample}(\alpha_5 v^2 + \alpha_6 \omega^2)$

5: $x' = x - \frac{\hat{v}}{\hat{\omega}} \sin\theta + \frac{\hat{v}}{\hat{\omega}} \sin(\theta + \hat{\omega}\Delta t)$

6: $y' = y + \frac{\hat{v}}{\hat{\omega}} \cos\theta - \frac{\hat{v}}{\hat{\omega}} \cos(\theta + \hat{\omega}\Delta t)$

7: $\theta' = \theta + \hat{\omega}\Delta t + \hat{\gamma}\Delta t$

8: *return* $x_t = (x', y', \theta')^T$

Table 5.3 Algorithm for sampling poses $x_t = (x' \ y' \ \theta')^T$ from a pose $x_{t-1} = (x \ y \ \theta)^T$ and a control $u_t = (v \ \omega)^T$. Note that we are perturbing the final orientation by an additional random term, $\hat{\gamma}$. The variables α_1 through α_6 are the parameters of the motion noise. The function **sample**(b^2) generates a random sample from a zero-centered distribution with variance b^2. It may, for example, be implemented using the algorithms in Table 5.4.

1: **Algorithm sample_normal_distribution**(b^2)**:**

2: *return* $\frac{1}{2} \sum_{i=1}^{12} \textbf{rand}(-b, b)$

3: **Algorithm sample_triangular_distribution**(b^2)**:**

4: *return* $\frac{\sqrt{6}}{2} [\textbf{rand}(-b, b) + \textbf{rand}(-b, b)]$

Table 5.4 Algorithm for sampling from (approximate) normal and triangular distributions with zero mean and variance b^2; see Winkler (1995: p293). The function **rand**(x, y) is assumed to be a pseudo random number generator with uniform distribution in $[x, y]$.

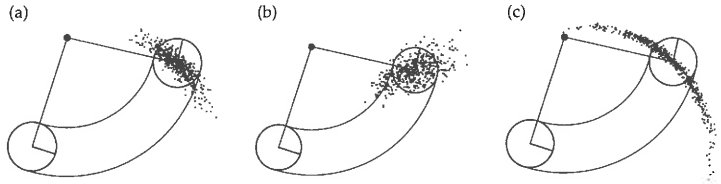

Figure 5.4 Sampling from the velocity motion model, using the same parameters as in Figure 5.3. Each diagram shows 500 samples.

new pose, in lines 5 through 7. Thus, the sampling procedure implements a simple physical robot motion model that incorporates control noise in its prediction, in just about the most straightforward way. Figure 5.4 illustrates the outcome of this sampling routine. It depicts 500 samples generated by **sample_motion_model_velocity**. The reader might want to compare this figure with the density depicted in Figure 5.3.

We note that in many cases, it is easier to sample x_t than calculate the density of a given x_t. This is because samples require only a forward simulation of the physical motion model. To compute the probability of a hypothetical pose amounts to retro-guessing of the error parameters, which requires us to calculate the inverse of the physical motion model. The fact that particle filters rely on sampling makes them specifically attractive from an implementation point of view.

5.3.3 Mathematical Derivation of the Velocity Motion Model

We will now derive the algorithms **motion_model_velocity** and **sample_motion_model_velocity**. As usual, the reader not interested in the mathematical details is invited to skip this section at first reading, and continue in Chapter 5.4 (page 132). The derivation begins with a generative model of robot motion, and then derives formulae for sampling and computing $p(x_t \mid u_t, x_{t-1})$ for arbitrary x_t, u_t, and x_{t-1}.

Exact Motion

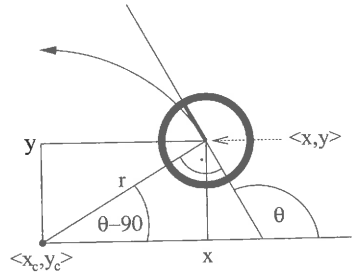

Figure 5.5 Motion carried out by a noise-free robot moving with constant velocities v and ω and starting at $(x\ y\ \theta)^T$.

Before turning to the probabilistic case, let us begin by stating the kinematics for an ideal, noise-free robot. Let $u_t = (v\ \omega)^T$ denote the control at time t. If both velocities are kept at a fixed value for the entire time interval $(t-1, t]$, the robot moves on a circle with radius

$$r = \left|\frac{v}{\omega}\right| \tag{5.5}$$

This follows from the general relationship between the translational and rotational velocities v and ω for an arbitrary object moving on a circular trajectory with radius r:

$$v = \omega \cdot r \tag{5.6}$$

Equation (5.5) encompasses the case where the robot does not turn at all (i.e., $\omega = 0$), in which case the robot moves on a straight line. A straight line corresponds to a circle with infinite radius, hence we note that r may be infinite.

Let $x_{t-1} = (x, y, \theta)^T$ be the initial pose of the robot, and suppose we keep the velocity constant at $(v\ \omega)^T$ for some time Δt. As one easily shows, the center of the circle is at

$$x_c = x - \frac{v}{\omega}\sin\theta \tag{5.7}$$

$$y_c = y + \frac{v}{\omega}\cos\theta \tag{5.8}$$

The variables $(x_c\ y_c)^T$ denote this coordinate. After Δt time of motion, our ideal robot will be at $x_t = (x', y', \theta')^T$ with

$$\begin{pmatrix} x' \\ y' \\ \theta' \end{pmatrix} = \begin{pmatrix} x_c + \frac{v}{\omega}\sin(\theta + \omega\Delta t) \\ y_c - \frac{v}{\omega}\cos(\theta + \omega\Delta t) \\ \theta + \omega\Delta t \end{pmatrix} \tag{5.9}$$

$$= \begin{pmatrix} x \\ y \\ \theta \end{pmatrix} + \begin{pmatrix} -\frac{v}{\omega}\sin\theta + \frac{v}{\omega}\sin(\theta + \omega\Delta t) \\ \frac{v}{\omega}\cos\theta - \frac{v}{\omega}\cos(\theta + \omega\Delta t) \\ \omega\Delta t \end{pmatrix}$$

The derivation of this expression follows from simple trigonometry: After Δt units of time, the noise-free robot has progressed $v \cdot \Delta t$ along the circle, which caused its heading direction to turn by $\omega \cdot \Delta t$. At the same time, its x and y coordinate is given by the intersection of the circle about $(x_c\ y_c)^T$, and the ray starting at $(x_c\ y_c)^T$ at the angle perpendicular to $\omega \cdot \Delta t$. The second transformation simply substitutes (5.8) into the resulting motion equations.

Of course, real robots cannot jump from one velocity to another, and keep velocity constant in each time interval. To compute the kinematics with non-constant velocities, it is therefore common practice to use small values for Δt, and to approximate the actual velocity by a constant within each time interval. The (approximate) final pose is then obtained by concatenating the corresponding cyclic trajectories using the mathematical equations just stated.

Real Motion

In reality, robot motion is subject to noise. The actual velocities differ from the commanded ones (or measured ones, if the robot possesses a sensor for measuring velocity). We will model this difference by a zero-centered random variable with finite variance. More precisely, let us assume the actual velocities are given by

$$\begin{pmatrix} \hat{v} \\ \hat{\omega} \end{pmatrix} = \begin{pmatrix} v \\ \omega \end{pmatrix} + \begin{pmatrix} \varepsilon_{\alpha_1 v^2 + \alpha_2 \omega^2} \\ \varepsilon_{\alpha_3 v^2 + \alpha_4 \omega^2} \end{pmatrix} \tag{5.10}$$

Here ε_{b^2} is a zero-mean error variable with variance b^2. Thus, the true velocity equals the commanded velocity plus some small, additive error (noise). In our model, the standard deviation of the error is proportional to the commanded velocity. The parameters α_1 to α_4 (with $\alpha_i \geq 0$ for $i = 1, \ldots, 4$) are robot-specific error parameters. They model the accuracy of the robot. The less accurate a robot, the larger these parameters.

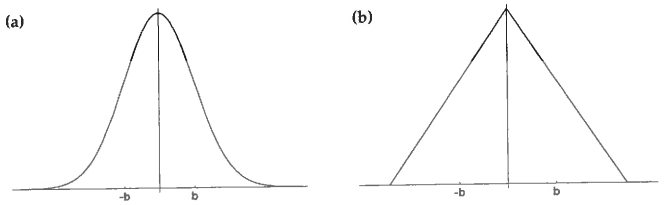

Figure 5.6 Probability density functions with variance b^2: (a) Normal distribution, (b) triangular distribution.

Two common choices for the error ε_{b^2} are the normal and the triangular distribution.

NORMAL DISTRIBUTION

The *normal distribution* with zero mean and variance b^2 is given by the density function

$$\varepsilon_{b^2}(a) = \frac{1}{\sqrt{2\pi\, b^2}}\, e^{-\frac{1}{2}\frac{a^2}{b^2}} \tag{5.11}$$

Figure 5.6a shows the density function of a normal distribution with variance b^2. Normal distributions are commonly used to model noise in continuous stochastic processes. Its support, which is the set of points a with $p(a) > 0$, is $\Re$.

TRIANGULAR DISTRIBUTION

The density of a *triangular distribution* with zero mean and variance b^2 is given by

$$\varepsilon_{b^2}(a) = \max\left\{0, \frac{1}{\sqrt{6}\, b} - \frac{|a|}{6\, b^2}\right\} \tag{5.12}$$

which is non-zero only in $(-\sqrt{6}b; \sqrt{6}b)$. As Figure 5.6b suggests, the density resembles the shape of a symmetric triangle—hence the name.

A better model of the actual pose $x_t = (x' \;\; y' \;\; \theta')^T$ after executing the motion command $u_t = (v \;\; \omega)^T$ at $x_{t-1} = (x \;\; y \;\; \theta)^T$ is thus

$$\begin{pmatrix} x' \\ y' \\ \theta' \end{pmatrix} = \begin{pmatrix} x \\ y \\ \theta \end{pmatrix} + \begin{pmatrix} -\frac{\hat{v}}{\hat{\omega}}\sin\theta + \frac{\hat{v}}{\hat{\omega}}\sin(\theta + \hat{\omega}\Delta t) \\ \frac{\hat{v}}{\hat{\omega}}\cos\theta - \frac{\hat{v}}{\hat{\omega}}\cos(\theta + \hat{\omega}\Delta t) \\ \hat{\omega}\Delta t \end{pmatrix} \tag{5.13}$$

This equation is obtained by substituting the commanded velocity $u_t = (v \;\; \omega)^T$ with the noisy motion $(\hat{v} \;\; \hat{\omega})^T$ in (5.9). However, this model is still not very realistic, for reasons discussed in turn.

Final Orientation

The two equations given above exactly describe the final location of the robot given that the robot actually moves on an exact circular trajectory with radius $r = \frac{\hat{v}}{\hat{\omega}}$. While the radius of this circular segment and the distance traveled is influenced by the control noise, the very fact that the trajectory is circular is not. The assumption of circular motion leads to an important degeneracy. In particular, the support of the density $p(x_t \mid u_t, x_{t-1})$ is two-dimensional, within a three-dimensional embedding pose space. The fact that all posterior poses are located on a two-dimensional manifold within the three-dimensional pose space is a direct consequence of the fact that we used only two noise variables, one for v and one for ω. Unfortunately, this degeneracy has important ramifications when applying Bayes filters for state estimation.

In reality, any meaningful posterior distribution is of course not degenerate, and poses can be found within a three-dimensional space of variations in x, y, and θ. To generalize our motion model accordingly, we will assume that the robot performs a rotation $\hat{\gamma}$ when it arrives at its final pose. Thus, instead of computing θ' according to (5.13), we model the final orientation by

$$\theta' = \theta + \hat{\omega}\Delta t + \hat{\gamma}\Delta t \tag{5.14}$$

with

$$\hat{\gamma} = \varepsilon_{\alpha_5 v^2 + \alpha_6 \omega^2} \tag{5.15}$$

Here α_5 and α_6 are additional robot-specific parameters that determine the variance of the additional rotational noise. Thus, the resulting motion model is as follows:

$$\begin{pmatrix} x' \\ y' \\ \theta' \end{pmatrix} = \begin{pmatrix} x \\ y \\ \theta \end{pmatrix} + \begin{pmatrix} -\frac{\hat{v}}{\hat{\omega}}\sin\theta + \frac{\hat{v}}{\hat{\omega}}\sin(\theta + \hat{\omega}\Delta t) \\ \frac{\hat{v}}{\hat{\omega}}\cos\theta - \frac{\hat{v}}{\hat{\omega}}\cos(\theta + \hat{\omega}\Delta t) \\ \hat{\omega}\Delta t + \hat{\gamma}\Delta t \end{pmatrix} \tag{5.16}$$

Computation of $p(x_t \mid u_t, x_{t-1})$

The algorithm **motion_model_velocity** in Table 5.1 implements the computation of $p(x_t \mid u_t, x_{t-1})$ for given values of $x_{t-1} = (x \;\; y \;\; \theta)^T$, $u_t = (v \;\; \omega)^T$, and $x_t = (x' \;\; y' \;\; \theta')^T$. The derivation of this algorithm is somewhat involved, as it effectively implements an inverse motion model. In particular, **motion_model_velocity** determines motion parameters $\hat{u}_t = (\hat{v} \;\; \hat{\omega})^T$ from the

poses x_{t-1} and x_t, along with an appropriate final rotation $\hat{\gamma}$. Our derivation makes it obvious as to why a final rotation is needed: For almost all values of x_{t-1}, u_t, and x_t, the motion probability would simply be zero without allowing for a final rotation.

Let us calculate the probability $p(x_t \mid u_t, x_{t-1})$ of control action $u_t = (v\ \omega)^T$ carrying the robot from the pose $x_{t-1} = (x\ y\ \theta)^T$ to the pose $x_t = (x'\ y'\ \theta')^T$ within Δt time units. To do so, we will first determine the control $\hat{u} = (\hat{v}\ \hat{\omega})^T$ required to carry the robot from x_{t-1} to position $(x'\ y')$, regardless of the robot's final orientation. Subsequently, we will determine the final rotation $\hat{\gamma}$ necessary for the robot to attain the orientation θ'. Based on these calculations, we can then easily calculate the desired probability $p(x_t \mid u_t, x_{t-1})$.

The reader may recall that our model assumes that the robot travels with a fixed velocity during Δt, resulting in a circular trajectory. For a robot that moved from $x_{t-1} = (x\ y\ \theta)^T$ to $x_t = (x'\ y')^T$, the center of the circle is defined as $(x^*\ y^*)^T$ and given by

$$\text{(5.17)} \quad \begin{pmatrix} x^* \\ y^* \end{pmatrix} = \begin{pmatrix} x \\ y \end{pmatrix} + \begin{pmatrix} -\lambda \sin\theta \\ \lambda \cos\theta \end{pmatrix} = \begin{pmatrix} \frac{x+x'}{2} + \mu(y-y') \\ \frac{y+y'}{2} + \mu(x'-x) \end{pmatrix}$$

for some unknown $\lambda, \mu \in \Re$. The first equality is the result of the fact that the circle's center is orthogonal to the initial heading direction of the robot; the second is a straightforward constraint that the center of the circle lies on a ray that lies on the half-way point between $(x\ y)^T$ and $(x'\ y')^T$ and is orthogonal to the line between these coordinates.

Usually, Equation (5.17) has a unique solution—except in the degenerate case of $\omega = 0$, in which the center of the circle lies at infinity. As the reader might want to verify, the solution is given by

$$\text{(5.18)} \quad \mu = \frac{1}{2} \frac{(x-x')\cos\theta + (y-y')\sin\theta}{(y-y')\cos\theta - (x-x')\sin\theta}$$

and hence

$$\text{(5.19)} \quad \begin{pmatrix} x^* \\ y^* \end{pmatrix} = \begin{pmatrix} \frac{x+x'}{2} + \frac{1}{2} \frac{(x-x')\cos\theta + (y-y')\sin\theta}{(y-y')\cos\theta - (x-x')\sin\theta} (y-y') \\ \frac{y+y'}{2} + \frac{1}{2} \frac{(x-x')\cos\theta + (y-y')\sin\theta}{(y-y')\cos\theta - (x-x')\sin\theta} (x'-x) \end{pmatrix}$$

The radius of the circle is now given by the Euclidean distance

$$\text{(5.20)} \quad r^* = \sqrt{(x-x^*)^2 + (y-y^*)^2} = \sqrt{(x'-x^*)^2 + (y'-y^*)^2}$$

Furthermore, we can now calculate the change of heading direction

$$\text{(5.21)} \quad \Delta\theta = \text{atan2}(y'-y^*, x'-x^*) - \text{atan2}(y-y^*, x-x^*)$$

Here atan2 is the common extension of the arcus tangens of y/x extended to the $\Re^2$ (most programming languages provide an implementation of this function):

$$\text{(5.22)} \quad \text{atan2}(y,x) = \begin{cases} \text{atan}(y/x) & \text{if } x > 0 \\ \text{sign(y)}\ (\pi - \text{atan}(|\text{y/x}|)) & \text{if } x < 0 \\ 0 & \text{if } x = y = 0 \\ \text{sign(y)}\ \pi/2 & \text{if } x = 0, y \neq 0 \end{cases}$$

Since we assume that the robot follows a circular trajectory, the translational distance between x_t and x_{t-1} along this circle is

$$\text{(5.23)} \quad \Delta\text{dist} = r^* \cdot \Delta\theta$$

From Δdist and $\Delta\theta$, it is now easy to compute the velocities $\hat{v}$ and $\hat{\omega}$:

$$\text{(5.24)} \quad \hat{u}_t = \begin{pmatrix} \hat{v} \\ \hat{\omega} \end{pmatrix} = \Delta t^{-1} \begin{pmatrix} \Delta\text{dist} \\ \Delta\theta \end{pmatrix}$$

The rotational velocity $\hat{\gamma}$ needed to achieve the final heading θ' of the robot in $(x'y')$ within Δt can be determined according to (5.14) as:

$$\text{(5.25)} \quad \hat{\gamma} = \Delta t^{-1}(\theta' - \theta) - \hat{\omega}$$

The *motion error* is the deviation of $\hat{u}_t$ and $\hat{\gamma}$ from the commanded velocity $u_t = (v\ \omega)^T$ and $\gamma = 0$, as defined in Equations (5.24) and (5.25).

$$\text{(5.26)} \quad v_{\text{err}} = v - \hat{v}$$
$$\text{(5.27)} \quad \omega_{\text{err}} = \omega - \hat{\omega}$$
$$\text{(5.28)} \quad \gamma_{\text{err}} = \hat{\gamma}$$

Under our error model, specified in Equations (5.10), and (5.15), these errors have the following probabilities:

$$\text{(5.29)} \quad \varepsilon_{\alpha_1 v^2 + \alpha_2 \omega^2}(v_{\text{err}})$$
$$\text{(5.30)} \quad \varepsilon_{\alpha_3 v^2 + \alpha_4 \omega^2}(\omega_{\text{err}})$$
$$\text{(5.31)} \quad \varepsilon_{\alpha_5 v^2 + \alpha_6 \omega^2}(\gamma_{\text{err}})$$

where ε_{b^2} denotes a zero-mean error variable with variance b^2, as before. Since we assume independence between the different sources of error, the desired probability $p(x_t \mid u_t, x_{t-1})$ is the product of these individual errors:

$$\text{(5.32)} \quad p(x_t \mid u_t, x_{t-1}) = \varepsilon_{\alpha_1 v^2 + \alpha_2 \omega^2}(v_{\text{err}}) \cdot \varepsilon_{\alpha_3 v^2 + \alpha_4 \omega^2}(\omega_{\text{err}}) \cdot \varepsilon_{\alpha_5 v^2 + \alpha_6 \omega^2}(\gamma_{\text{err}})$$

To see the correctness of the algorithm **motion_model_velocity** in Table 5.1, the reader may notice that this algorithm implements this expression. More specifically, lines 2 to 9 are equivalent to Equations (5.18), (5.19), (5.20), (5.21), (5.24), and (5.25). Line 10 implements (5.32), substituting the error terms as specified in Equations (5.29) to (5.31).

Sampling from $p(x' \mid u, x)$

The sampling algorithm **sample_motion_model_velocity** in Table 5.3 implements a forward model, as discussed earlier in this section. Lines 5 through 7 correspond to Equation (5.16). The noisy values calculated in lines 2 through 4 correspond to Equations (5.10) and (5.15).

The algorithm **sample_normal_distribution** in Table 5.4 implements a common approximation to sampling from a normal distribution. This approximation exploits the central limit theorem, which states that any average of non-degenerate random variables converges to a normal distribution. By averaging 12 uniform distributions, **sample_normal_distribution** generates values that are approximately normal distributed; though technically the resulting values lie always in $[-2b, 2b]$. Finally, **sample_triangular_distribution** in Table 5.4 implements a sampler for triangular distributions.

5.4 Odometry Motion Model

The velocity motion model discussed thus far uses the robot's velocity to compute posteriors over poses. Alternatively, one might want to use the odometry measurements as the basis for calculating the robot's motion over time. Odometry is commonly obtained by integrating wheel encoder information; most commercial robots make such integrated pose estimation available in periodic time intervals (e.g., every tenth of a second). This leads to a second motion model discussed in this chapter, the *odometry motion model*. The odometry motion model uses odometry measurements in lieu of controls.

Practical experience suggests that odometry, while still erroneous, is usually more accurate than velocity. Both suffer from drift and slippage, but velocity additionally suffers from the mismatch between the actual motion controllers and its (crude) mathematical model. However, odometry is only available in retrospect, after the robot moved. This poses no problem for filter algorithms, such as the localization and mapping algorithms discussed in later chapters. But it makes this information unusable for accurate motion planning and control.

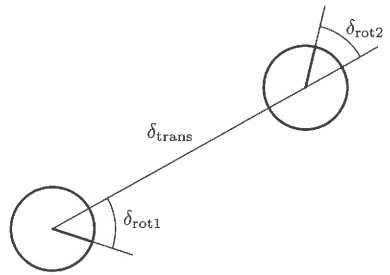

Figure 5.7 Odometry model: The robot motion in the time interval $(t-1, t]$ is approximated by a rotation δ_{rot1}, followed by a translation δ_{trans} and a second rotation δ_{rot2}. The turns and translations are noisy.

5.4.1 Closed Form Calculation

Technically, odometric information are sensor measurements, not controls. To model odometry as measurements, the resulting Bayes filter would have to include the actual velocity as state variables—which increases the dimension of the state space. To keep the state space small, it is therefore common to consider odometry data as if it were control signals. In this section, we will treat odometry measurements just like controls. The resulting model is at the core of many of today's best probabilistic robot systems.

Let us define the format of our control information. At time t, the correct pose of the robot is modeled by the random variable x_t. The robot odometry estimates this pose; however, due to drift and slippage there is no fixed coordinate transformation between the coordinates used by the robot's internal odometry and the physical world coordinates. In fact, knowing this transformation would solve the robot localization problem!

The odometry model uses the *relative motion information*, as measured by the robot's internal odometry. More specifically, in the time interval $(t-1, t]$, the robot advances from a pose x_{t-1} to pose x_t. The odometry reports back to us a related advance from $\bar{x}_{t-1} = (\bar{x} \;\; \bar{y} \;\; \bar{\theta})^T$ to $\bar{x}_t = (\bar{x}' \;\; \bar{y}' \;\; \bar{\theta}')^T$. Here the

1: **Algorithm motion_model_odometry**(x_t, u_t, x_{t-1})**:**

2: $\delta_{\text{rot1}} = \text{atan2}(\bar{y}' - \bar{y}, \bar{x}' - \bar{x}) - \bar{\theta}$
3: $\delta_{\text{trans}} = \sqrt{(\bar{x} - \bar{x}')^2 + (\bar{y} - \bar{y}')^2}$
4: $\delta_{\text{rot2}} = \bar{\theta}' - \bar{\theta} - \delta_{\text{rot1}}$

5: $\hat{\delta}_{\text{rot1}} = \text{atan2}(y' - y, x' - x) - \theta$
6: $\hat{\delta}_{\text{trans}} = \sqrt{(x - x')^2 + (y - y')^2}$
7: $\hat{\delta}_{\text{rot2}} = \theta' - \theta - \hat{\delta}_{\text{rot1}}$

8: $p_1 = \textbf{prob}(\delta_{\text{rot1}} - \hat{\delta}_{\text{rot1}}, \alpha_1 \hat{\delta}^2_{\text{rot1}} + \alpha_2 \hat{\delta}^2_{\text{trans}})$
9: $p_2 = \textbf{prob}(\delta_{\text{trans}} - \hat{\delta}_{\text{trans}}, \alpha_3 \hat{\delta}^2_{\text{trans}} + \alpha_4 \hat{\delta}^2_{\text{rot1}} + \alpha_4 \hat{\delta}^2_{\text{rot2}})$
10: $p_3 = \textbf{prob}(\delta_{\text{rot2}} - \hat{\delta}_{\text{rot2}}, \alpha_1 \hat{\delta}^2_{\text{rot2}} + \alpha_2 \hat{\delta}^2_{\text{trans}})$

11: *return* $p_1 \cdot p_2 \cdot p_3$

Table 5.5 Algorithm for computing $p(x_t \mid u_t, x_{t-1})$ based on odometry information. Here the control u_t is given by $(\bar{x}_{t-1} \ \bar{x}_t)^T$, with $\bar{x}_{t-1} = (\bar{x} \ \bar{y} \ \bar{\theta})$ and $\bar{x}_t = (\bar{x}' \ \bar{y}' \ \bar{\theta}')$.

bar indicates that these are odometry measurements embedded in a robot-internal coordinate whose relation to the global world coordinates is unknown. The key insight for utilizing this information in state estimation is that the relative difference between $\bar{x}_{t-1}$ and $\bar{x}_t$, under an appropriate definition of the term "difference," is a good estimator for the difference of the true poses x_{t-1} and x_t. The motion information u_t is, thus, given by the pair

$$u_t = \begin{pmatrix} \bar{x}_{t-1} \\ \bar{x}_t \end{pmatrix} \tag{5.33}$$

To extract relative odometry, u_t is transformed into a sequence of three steps: a rotation, followed by a straight line motion (translation), and another rotation. Figure 5.7 illustrates this decomposition: the initial turn is called δ_{rot1}, the translation δ_{trans}, and the second rotation δ_{rot2}. As the reader easily verifies, each pair of positions $(\bar{s} \ \bar{s}')$ has a unique parameter vector $(\delta_{\text{rot1}} \ \delta_{\text{trans}} \ \delta_{\text{rot2}})^T$, and these parameters are sufficient to reconstruct the

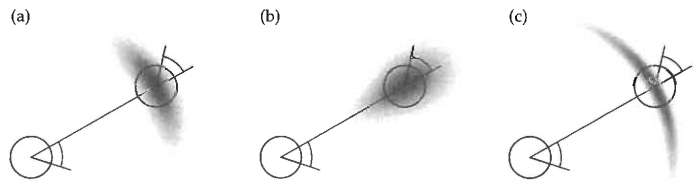

Figure 5.8 The odometry motion model, for different noise parameter settings.

relative motion between $\bar{s}$ and $\bar{s}'$. Thus, $\delta_{\text{rot1}}, \delta_{\text{trans}}, \delta_{\text{rot2}}$ form together a sufficient statistics of the relative motion encoded by the odometry.

The probabilistic motion model assumes that these three parameters are corrupted by independent noise. The reader may note that odometry motion uses one more parameter than the velocity vector defined in the previous section, for which reason we will not face the same degeneracy that led to the definition of a "final rotation."

Before delving into mathematical detail, let us state the basic algorithm for calculating this density in closed form. Table 5.5 depicts the algorithm for computing $p(x_t \mid u_t, x_{t-1})$ from odometry. This algorithm accepts as an input an initial pose x_{t-1}, a pair of poses $u_t = (\bar{x}_{t-1} \ \bar{x}_t)^T$ obtained from the robot's odometry, and a hypothesized final pose x_t. It outputs the numerical probability $p(x_t \mid u_t, x_{t-1})$.

Lines 2 to 4 in Table 5.5 recover relative motion parameters $(\delta_{\text{rot1}} \ \delta_{\text{trans}} \ \delta_{\text{rot2}})^T$ from the odometry readings. As before, they implement an *inverse motion model*. The corresponding relative motion parameters $(\hat{\delta}_{\text{rot1}} \ \hat{\delta}_{\text{trans}} \ \hat{\delta}_{\text{rot2}})^T$ for the given poses x_{t-1} and x_t are calculated in lines 5 through 7 of this algorithm. Lines 8 to 10 compute the error probabilities for the individual motion parameters. As above, the function $\textbf{prob}(a, b^2)$ implements an error distribution over a with zero mean and variance b^2. Here the implementer must observe that all angular differences must lie in $[-\pi, \pi]$. Hence the outcome of $\delta_{\text{rot2}} - \bar{\delta}_{\text{rot2}}$ has to be truncated correspondingly—a common error that tends to be difficult to debug. Finally, line 11 returns the combined error probability, obtained by multiplying the individual error probabilities p_1, p_2, and p_3. This last step assumes independence between the different error sources. The variables α_1 through α_4 are robot-specific parameters that specify the noise in robot motion.

1: **Algorithm sample_motion_model_odometry**(u_t, x_{t-1})**:**

2: $\delta_{\text{rot1}} = \text{atan2}(\bar{y}' - \bar{y}, \bar{x}' - \bar{x}) - \bar{\theta}$
3: $\delta_{\text{trans}} = \sqrt{(\bar{x} - \bar{x}')^2 + (\bar{y} - \bar{y}')^2}$
4: $\delta_{\text{rot2}} = \bar{\theta}' - \bar{\theta} - \delta_{\text{rot1}}$

5: $\hat{\delta}_{\text{rot1}} = \delta_{\text{rot1}} - \textbf{sample}(\alpha_1 \delta^2_{\text{rot1}} + \alpha_2 \delta^2_{\text{trans}})$
6: $\hat{\delta}_{\text{trans}} = \delta_{\text{trans}} - \textbf{sample}(\alpha_3 \delta^2_{\text{trans}} + \alpha_4\, \delta^2_{\text{rot1}} + \alpha_4\, \delta^2_{\text{rot2}})$
7: $\hat{\delta}_{\text{rot2}} = \delta_{\text{rot2}} - \textbf{sample}(\alpha_1 \delta^2_{\text{rot2}} + \alpha_2 \delta^2_{\text{trans}})$

8: $x' = x + \hat{\delta}_{\text{trans}}\, \cos(\theta + \hat{\delta}_{\text{rot1}})$
9: $y' = y + \hat{\delta}_{\text{trans}}\, \sin(\theta + \hat{\delta}_{\text{rot1}})$
10: $\theta' = \theta + \hat{\delta}_{\text{rot1}} + \hat{\delta}_{\text{rot2}}$

11: *return* $x_t = (x', y', \theta')^T$

Table 5.6 Algorithm for sampling from $p(x_t \mid u_t, x_{t-1})$ based on odometry information. Here the pose at time t is represented by $x_{t-1} = (x\ y\ \theta)^T$. The control is a differentiable set of two pose estimates obtained by the robot's odometer, $u_t = (\bar{x}_{t-1}\ \bar{x}_t)^T$, with $\bar{x}_{t-1} = (\bar{x}\ \bar{y}\ \bar{\theta})$ and $\bar{x}_t = (\bar{x}'\ \bar{y}'\ \bar{\theta}')$.

Figure 5.8 shows examples of our odometry motion model for different values of the error parameters α_1 to α_4. The distribution in Figure 5.8a is a typical one, whereas the ones shown in Figures 5.8b and 5.8c indicate unusually large translational and rotational errors, respectively. The reader may want to carefully compare these diagrams with those in Figure 5.3 on page 122. The smaller the time between two consecutive measurements, the more similar those different motion models. Thus, if the belief is updated frequently e.g., every tenth of a second for a conventional indoor robot, the difference between these motion models is not very significant.

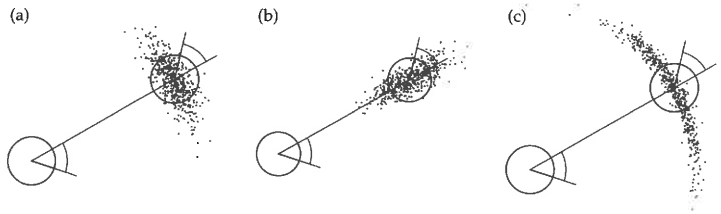

Figure 5.9 Sampling from the odometry motion model, using the same parameters as in Figure 5.8. Each diagram shows 500 samples.

5.4.2 Sampling Algorithm

If particle filters are used for localization, we would also like to have an algorithm for *sampling* from $p(x_t \mid u_t, x_{t-1})$. Recall that particle filters (Chapter 4.3) require samples of $p(x_t \mid u_t, x_{t-1})$, rather than a closed-form expression for computing $p(x_t \mid u_t, x_{t-1})$ for any x_{t-1}, u_t, and x_t. The algorithm **sample_motion_model_odometry**, shown in Table 5.6, implements the sampling approach. It accepts an initial pose x_{t-1} and an odometry reading u_t as input, and outputs a random x_t distributed according to $p(x_t \mid u_t, x_{t-1})$. It differs from the previous algorithm in that it randomly guesses a pose x_t (lines 5-10), instead of computing the probability of a given x_t. As before, the sampling algorithm **sample_motion_model_odometry** is somewhat easier to implement than the closed-form algorithm **motion_model_odometry**, since it side-steps the need for an inverse model.

Figure 5.9 shows examples of sample sets generated by **sample_motion_model_odometry**, using the same parameters as in the model shown in Figure 5.8. Figure 5.10 illustrates the motion model "in action" by superimposing sample sets from multiple time steps. This data has been generated using the motion update equations of the algorithm **particle_filter** (Table 4.3), assuming the robot's odometry follows the path indicated by the solid line. The figure illustrates how the uncertainty grows as the robot moves. The samples are spread across an increasingly large space.

5.4.3 Mathematical Derivation of the Odometry Motion Model

The derivation of the algorithms is relatively straightforward, and once again may be skipped at first reading. To derive a probabilistic motion model using

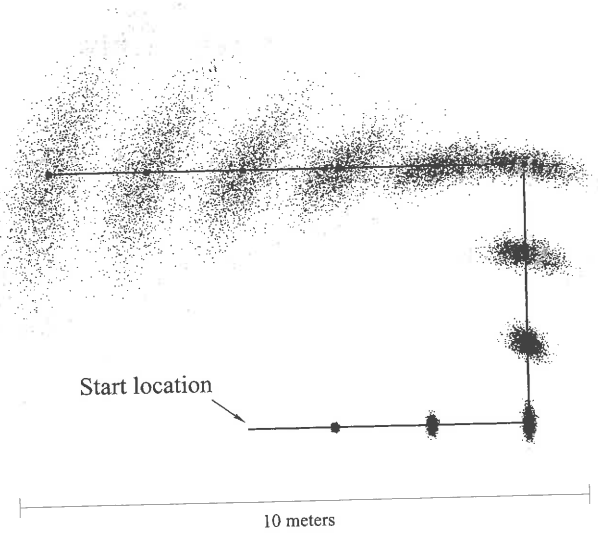

Figure 5.10 Sampling approximation of the position belief for a non-sensing robot. The solid line displays the actions, and the samples represent the robot's belief at different points in time.

odometry, we recall that the relative difference between any two poses is represented by a concatenation of three basic motions: a rotation, a straight-line motion (translation), and another rotation. The following equations show how to calculate the values of the two rotations and the translation from the odometry reading $u_t = (\bar{x}_{t-1}\ \bar{x}_t)^T$, with $\bar{x}_{t-1} = (\bar{x}\ \bar{y}\ \bar{\theta})$ and $\bar{x}_t = (\bar{x}'\ \bar{y}'\ \bar{\theta}')$:

$$\delta_{\text{rot1}} = \text{atan2}(\bar{y}' - \bar{y}, \bar{x}' - \bar{x}) - \bar{\theta} \tag{5.34}$$

$$\delta_{\text{trans}} = \sqrt{(\bar{x} - \bar{x}')^2 + (\bar{y} - \bar{y}')^2} \tag{5.35}$$

$$\delta_{\text{rot2}} = \bar{\theta}' - \bar{\theta} - \delta_{\text{rot1}} \tag{5.36}$$

To model the motion error, we assume that the "true" values of the rotation and translation are obtained from the measured ones by subtracting independent noise ε_{b^2} with zero mean and variance b^2:

$$\hat{\delta}_{\text{rot1}} = \delta_{\text{rot1}} - \varepsilon_{\alpha_1 \delta^2_{\text{rot1}} + \alpha_2 \delta^2_{\text{trans}}} \tag{5.37}$$

$$\hat{\delta}_{\text{trans}} = \delta_{\text{trans}} - \varepsilon_{\alpha_3 \delta^2_{\text{trans}} + \alpha_4 \delta^2_{\text{rot1}} + \alpha_4 \delta^2_{\text{rot2}}} \tag{5.38}$$

$$\hat{\delta}_{\text{rot2}} = \delta_{\text{rot2}} - \varepsilon_{\alpha_1 \delta^2_{\text{rot2}} + \alpha_2 \delta^2_{\text{trans}}} \tag{5.39}$$

As in the previous section, ε_{b^2} is a zero-mean noise variable with variance b^2. The parameters α_1 to α_4 are robot-specific error parameters, which specify the error accrued with motion.

Consequently, the true position, x_t, is obtained from x_{t-1} by an initial rotation with angle $\hat{\delta}_{\text{rot1}}$, followed by a translation with distance $\hat{\delta}_{\text{trans}}$, followed by another rotation with angle $\hat{\delta}_{\text{rot2}}$. Thus,

$$\begin{pmatrix} x' \\ y' \\ \theta' \end{pmatrix} = \begin{pmatrix} x \\ y \\ \theta \end{pmatrix} + \begin{pmatrix} \hat{\delta}_{\text{trans}} \cos(\theta + \hat{\delta}_{\text{rot1}}) \\ \hat{\delta}_{\text{trans}} \sin(\theta + \hat{\delta}_{\text{rot1}}) \\ \hat{\delta}_{\text{rot1}} + \hat{\delta}_{\text{rot2}} \end{pmatrix} \tag{5.40}$$

Notice that algorithm **sample_motion_model_odometry** implements Equations (5.34) through (5.40).

The algorithm **motion_model_odometry** is obtained by noticing that lines 5-7 compute the motion parameters $\hat{\delta}_{\text{rot1}}$, $\hat{\delta}_{\text{trans}}$, and $\hat{\delta}_{\text{rot2}}$ for the hypothesized pose x_t, relative to the initial pose x_{t-1}. The difference of both,

$$\delta_{\text{rot1}} - \hat{\delta}_{\text{rot1}} \tag{5.41}$$

$$\delta_{\text{trans}} - \hat{\delta}_{\text{trans}} \tag{5.42}$$

$$\delta_{\text{rot2}} - \hat{\delta}_{\text{rot2}} \tag{5.43}$$

is the *error* in odometry, assuming of course that x_t is the true final pose. The error model (5.37) to (5.39) implies that the probability of these errors is given by

$$p_1 = \varepsilon_{\alpha_1 \delta^2_{\text{rot1}} + \alpha_2 \delta^2_{\text{trans}}}(\delta_{\text{rot1}} - \hat{\delta}_{\text{rot1}}) \tag{5.44}$$

$$p_2 = \varepsilon_{\alpha_3 \delta^2_{\text{trans}} + \alpha_4 \delta^2_{\text{rot1}} + \alpha_4 \delta^2_{\text{rot2}}}(\delta_{\text{trans}} - \hat{\delta}_{\text{trans}}) \tag{5.45}$$

$$p_3 = \varepsilon_{\alpha_1 \delta^2_{\text{rot2}} + \alpha_2 \delta^2_{\text{trans}}}(\delta_{\text{rot2}} - \hat{\delta}_{\text{rot2}}) \tag{5.46}$$

with the distributions ε defined as above. These probabilities are computed in lines 8-10 of our algorithm **motion_model_odometry**, and since the errors are assumed to be independent, the joint error probability is the product $p_1 \cdot p_2 \cdot p_3$ (c.f., line 11).

5.5 Motion and Maps

By considering $p(x_t \mid u_t, x_{t-1})$, we defined robot motion in a vacuum. In particular, this model describes robot motion in the absence of any knowledge about the nature of the environment. In many cases, we are also given a map m, which may contain information pertaining to the places that a robot may or may not be able to navigate. For example, *occupancy maps*, which will be explained in Chapter 9, distinguish *free* (traversable) from *occupied* terrain. The robot's pose must always be in the free space. Therefore, knowing m gives us further information about the robot pose x_t before, during, and after executing a control u_t.

This consideration calls for a motion model that takes the map m into account. We will denote this model by $p(x_t \mid u_t, x_{t-1}, m)$, indicating that it considers the map m in addition to the standard variables. If m carries information relevant to pose estimation, we have

$$p(x_t \mid u_t, x_{t-1}) \neq p(x_t \mid u_t, x_{t-1}, m) \tag{5.47}$$

MAP-BASED MOTION MODEL

The motion model $p(x_t \mid u_t, x_{t-1}, m)$ should give better results than the map-free motion model $p(x_t \mid u_t, x_{t-1})$. We will refer to $p(x_t \mid u_t, x_{t-1}, m)$ as *map-based motion model*. The map-based motion model computes the likelihood that a robot placed in a world with map m arrives at pose x_t upon executing action u_t at pose x_{t-1}. Unfortunately, computing this motion model in closed form is difficult. This is because to compute the likelihood of being at x_t after executing action u_t, one has to incorporate the probability that an unoccupied path exists between x_{t-1} and x_t and that the robot might have followed this unoccupied path when executing the control u_t—a complex operation.

Luckily, there exists an efficient approximation for the map-based motion model, which works well if the distance between x_{t-1} and x_t is small (e.g., smaller than half a robot diameter). The approximation factorizes the map-based motion model into two components:

$$p(x_t \mid u_t, x_{t-1}, m) = \eta \frac{p(x_t \mid u_t, x_{t-1})\, p(x_t \mid m)}{p(x_t)} \tag{5.48}$$

where η is the usual normalizer. Usually, $p(x_t)$ is also uniform and can be subsumed into the constant normalizer. One then simply multiplies the map-free estimate $p(x_t \mid u_t, x_{t-1})$ with a second term, $p(x_t \mid m)$, which expresses the "consistency" of pose x_t with the map m. In the case of occupancy maps, $p(x_t \mid m) = 0$ if and only if the robot would be placed in an occupied grid cell


```
1:  Algorithm motion_model_with_map(x_t, u_t, x_{t-1}, m):
2:      return p(x_t | u_t, x_{t-1}) · p(x_t | m)

1:  Algorithm sample_motion_model_with_map(u_t, x_{t-1}, m):
2:      do
3:          x_t = sample_motion_model(u_t, x_{t-1})
3:          π = p(x_t | m)
4:      until π > 0
5:      return ⟨x_t, π⟩
```

Table 5.7 Algorithm for computing $p(x_t \mid u_t, x_{t-1}, m)$, which utilizes a map m of the environment. This algorithms bootstraps previous motion models (Tables 5.1, 5.3, 5.5, and 5.6) to models that take into account that robots cannot be placed in occupied space in the map m.

in the map; otherwise it assumes a constant value. By multiplying $p(x_t \mid m)$ and $p(x_t \mid u_t, x_{t-1})$, we obtain a distribution that assigns all probability mass to poses x_t consistent with the map, which otherwise has the same shape as $p(x_t \mid u_t, x_{t-1})$. As η can be computed by normalization, this approximation of a map-based motion model can be computed efficiently without any significant overhead compared to a map-free motion model.

Table 5.7 states the basic algorithms for computing and for sampling from the map-based motion model. Notice that the sampling algorithm returns a weighted sample, which includes an importance factor proportional to $p(x_t \mid m)$. Care has to be taken in the implementation of the sample version, to ensure termination of the inner loop. An example of the motion model is illustrated in Figure 5.11. The density in Figure 5.11a is $p(x_t \mid u_t, x_{t-1})$, computed according to the velocity motion model. Now suppose the map m possesses a long rectangular obstacle, as indicated in Figure 5.11b. The probability $p(x_t \mid m)$ is zero at all poses x_t where the robot would intersect the obstacle. Since our example robot is circular, this region is equivalent to the obstacle grown by a robot radius—this is equivalent to mapping the obstacle from *workspace* to the robot's *configuration space* or *pose space*. The resulting

CONFIGURATION SPACE

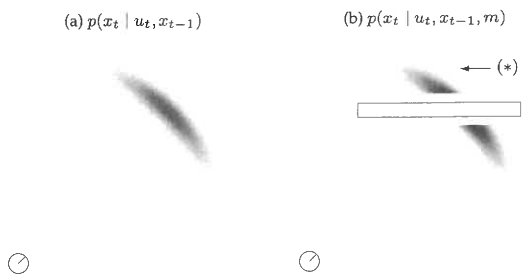

Figure 5.11 Velocity motion model (a) without a map and (b) conditioned on a map m.

probability $p(x_t \mid u_t, x_{t-1}, m)$, shown in Figure 5.11b, is the normalized product of $p(x_t \mid m)$ and $p(x_t \mid u_t, x_{t-1})$. It is zero in the extended obstacle area, and proportional to $p(x_t \mid u_t, x_{t-1})$ everywhere else.

Figure 5.11 also illustrates a problem with our approximation. The region marked $(*)$ possesses non-zero likelihood, since both $p(x_t \mid u_t, x_{t-1})$ and $p(x_t \mid m)$ are non-zero in this region. However, for the robot to be in this particular area it must have gone through the wall, which is impossible in the real world. This error is the result of checking model consistency at the final pose x_t only, instead of verifying the consistency of the robot's path to the goal. In practice, however, such errors only occur for relatively large motions u_t, and it can be neglected for higher update frequencies.

To shed light onto the nature of the approximation, let us briefly derive it. Equation (5.48) can be obtained by applying Bayes rule:

$$p(x_t \mid u_t, x_{t-1}, m) = \eta\, p(m \mid x_t, u_t, x_{t-1})\, p(x_t \mid u_t, x_{t-1}) \tag{5.49}$$

If we approximate $p(m \mid x_t, u_t, x_{t-1})$ by $p(m \mid x_t)$ and observe that $p(m)$ is a constant relative to the desired posterior, we obtain the desired equation as follows:

$$\begin{aligned} p(x_t \mid u_t, x_{t-1}, m) &= \eta\, p(m \mid x_t)\, p(x_t \mid u_t, x_{t-1}) \\ &= \eta\, \frac{p(x_t \mid m)\, p(m)}{p(x_t)}\, p(x_t \mid u_t, x_{t-1}) \\ &= \eta\, \frac{p(x_t \mid m)\, p(x_t \mid u_t, x_{t-1})}{p(x_t)} \end{aligned} \tag{5.50}$$

Here η is the normalizer (notice that the value of η is different for the different steps in our transformation). This brief analysis shows that our map-based model is justified under the rough assumption that

$$p(m \mid x_t, u_t, x_{t-1}) = p(m \mid x_t) \tag{5.51}$$

Obviously, these expressions are not equal. When computing the conditional over m, our approximation omits two terms: u_t and x_{t-1}. By omitting these terms, we discard any information relating to the robot's path leading up to x_t. All we know is that its final pose is x_t. We already noticed the consequences of this omission in our example above, when we observed that poses behind a wall may possess non-zero likelihood. Our approximate map-based motion model may falsely assume that the robot just went through a wall, as long as the initial and final poses are in the unoccupied space. How damaging can this be? As noted above, this depends on the update interval. In fact, for sufficiently high update rates, and assuming that the noise variables in the motion model are bounded, we can guarantee that the approximation is tight and this effect will not occur.

This analysis illustrates a subtle insight pertaining to the implementation of the algorithm. In particular, one has to pay attention to the update frequency. A Bayes filter that is updated frequently might yield fundamentally different results than one that is updated only occasionally.

5.6 Summary

This section derived the two principal probabilistic motion models for mobile robots operating on the plane.

- We derived an algorithm for the probabilistic motion model $p(x_t \mid u_t, x_{t-1})$ that represents control u_t by a translational and angular velocity, executed over a fixed time interval Δt. In implementing this model, we realized that two control noise parameters, one for the translational and one for the rotational velocity, are insufficient to generate a space-filling (non-generate) posterior. We therefore added a third noise parameter, expressed as a noisy "final rotation."

- We presented an alternative motion model that uses the robot's odometry as input. Odometric measurements were expressed by three parameters, an initial rotation, followed by a translation, and a final rotation. The probabilistic motion model was implemented by assuming that all three

of these parameters are subject to noise. We noted that odometry readings are technically not controls; however, by using them just like controls we arrived at a simpler formulation of the estimation problem.

- For both motion models, we presented two types of implementations, one in which the probability $p(x_t \mid u_t, x_{t-1})$ is calculated in closed form, and one that enables us to generate samples from $p(x_t \mid u_t, x_{t-1})$. The closed-form expression accepts as an input x_t, u_t, and x_{t-1}, and outputs a numerical probability value. To calculate this probability, the algorithms effectively invert the motion model, to compare the *actual* with the *commanded* control parameters. The sampling model does not require such an inversion. Instead, it implements a forward model of the motion model $p(x_t \mid u_t, x_{t-1})$. It accepts as an input the values u_t and x_{t-1} and outputs a random x_t drawn according to $p(x_t \mid u_t, x_{t-1})$. Closed-form models are required for some probabilistic algorithms. Others, most notably particle filters, utilize sampling models.

- Finally we extended all motion models to incorporate a map of the environment. The resulting probability $p(x_t \mid u_t, x_{t-1}, m)$ incorporates a map m in its conditional. This extension followed the intuition that the map specifies where a robot may be, which has an effect of the ability to move from pose x_{t-1} to x_t. The resulting algorithm was approximate, in that we only checked for the validity of the final pose.

The motion models discussed here are only examples: Clearly, the field of robotic actuators is much richer than just mobile robots operating in flat terrain. Even within the field of mobile robotics, there exist a number of devices that are not covered by the models discussed here. Examples include holonomic robots which can move sideways, or cars with suspension. Our description also does not consider robot dynamics, which are important for fast-moving vehicles such as cars on highways. Most of these robots can be modeled analogously; simply specify the physical laws of robot motion, and specify appropriate noise parameters. For dynamic models, this will require extending the robot state by a velocity vector that captures the dynamic state of the vehicle. In many ways, these extensions are straightforward.

As far as measuring ego-motion is concerned, many robots rely on inertial sensors to measure motion, as a supplement to or in place of odometry. Entire books have been dedicated to filter design using inertial sensors. Readers are encouraged to include richer models and sensors when odometry is insufficient.

5.7 Bibliographical Remarks

The present material extends the basic kinematic equations of specific types of mobile robots (Cox and Wilfong 1990) by a probabilistic component. Drives covered by our model are the differential drive, the Ackerman drive, and synchro-drive (Borenstein et al. 1996). Drive systems not covered by our model are those without non-holonomic constraints (Latombe 1991) like robots equipped with Mecanum wheels (Ilon 1975) or even legged robots, as described in pioneering papers by Raibert et al. (1986); Raibert (1991); Saranli and Koditschek (2002).

The field of robotics has studied robot motion and interaction with a robotic environment in much more depth. Contemporary *texts on mobile robots* covering aspects of kinematics and dynamics are due to Murphy (2000c); Dudek and Jenkin (2000); Siegwart and Nourbakhsh (2004). Cox and Wilfong (1990) provides a collection of articles by leading researchers at the time of publication; see also Kortenkamp et al. (1998). Classical treatments of robotic kinematics and dynamics can be found in Craig (1989); Vukobratović (1989); Paul (1981); and Yoshikawa (1990). A more modern text addressing robotic dynamics is the one by Featherstone (1987). Compliant motion as one form of environment interaction has been studied by Mason (2001). Terramechanics, which refers to the interaction of wheeled robots with the ground, has been studied in seminal texts by Bekker (1956, 1969) and Wong (1989). A contemporary text on wheel-ground interaction can be found in Iagnemma and Dubowsky (2004). Generalizing such models into a probabilistic framework is a promising direction for future research.

5.8 Exercises

DYNAMICS

1. All robot models in this chapter were kinematic. In this exercise, you will consider a robot with *dynamics*. Consider a robot that lives in a 1-D coordinate system. Its location will be denoted by x, its velocity by $\dot{x}$, and its acceleration by $\ddot{x}$. Suppose we can only control the acceleration $\ddot{x}$. Develop a mathematical motion model that computes the posterior over the pose x' and the velocity $\dot{x}'$ from an initial pose x and velocity $\dot{x}$, assuming that the acceleration $\ddot{x}$ is the sum of a commanded acceleration and a zero-mean Gaussian noise term with variance σ^2 (and assume that the actual acceleration remains constant in the simulation interval Δt). Are x' and $\dot{x}'$ correlated in the posterior? Explain why/why not.

2. Consider again the dynamic robot from Exercise 1. Provide a mathematical formula for computing the posterior distribution over the final velocity $\dot{x}'$, from the initial robot location x, the initial velocity $\dot{x}$, and the final pose x'. What is remarkable about this posterior?

3. Suppose we control this robot with random accelerations for T time intervals, for some large value of T. Will the final location x and the velocity $\dot{x}$ be correlated? If yes, will they be *fully* correlated as $T \uparrow \infty$, so that one variable becomes a deterministic function of the other?